



OPEN

SUBJECT AREAS:
FUEL CELLS
ELECTROCATALYSISReceived
30 October 2014Accepted
3 December 2014Published
5 January 2015Correspondence and
requests for materials
should be addressed to
Y.C. (ndchenyu@
gmail.com) or Y.T.
(tangyawen@njnu.
edu.cn)

A Strategy for Fabricating Porous PdNi@Pt Core-shell Nanostructures and Their Enhanced Activity and Durability for the Methanol Electrooxidation

Xinyu Liu¹, Guangrui Xu², Yu Chen², Tianhong Lu¹, Yawen Tang¹ & Wei Xing³

¹Jiangsu Key Laboratory of New Power Batteries, Jiangsu Collaborative Innovation Center of Biomedical Functional Materials, School of Chemistry and Materials Science, Nanjing Normal University, Nanjing 210023, P. R. China, ²School of Materials Science and Engineering, Shaanxi Normal University, Xi'an 710062, P. R. China, ³State Key Laboratory of Electroanalytical Chemistry, Changchun Institute of Applied Chemistry, Chinese Academy of Sciences, Changchun, Jilin 130022, P. R. China.

Three-dimensionally (3D) porous morphology of nanostructures can effectively improve their electrocatalytic activity and durability for various electrochemical reactions owing to big surface area and interconnected structure. Cyanogel, a jelly-like inorganic polymer, can be used to synthesize various three-dimensionally (3D) porous alloy nanomaterials owing to its double-metal property and particular 3D backbone. Here, 3D porous PdNi@Pt core-shell nanostructures (CSNSs) are facilely synthesized by first preparing the Pd-Ni alloy networks (Pd-Ni ANWs) core via cyanogel-reduction method followed by a galvanic displacement reaction to generate the Pt-rich shell. The as-synthesized PdNi@Pt CSNSs exhibit a much improved catalytic activity and durability for the methanol oxidation reaction (MOR) in the acidic media compared to the commercial used Pt black because of their specific structural characteristics. The facile and mild method described herein is highly attractive for the synthesis of 3D porous core-shell nanostructures.

Direct methanol fuel cells (DMFCs), a green low-temperature power source, have wide applications in portable electronic devices, residence and automobiles because of their low pollution level, high energy efficiency, convenient storage and transportation, and clean utilization^{1–8}. However, the realization and commercialization of DMFCs have been challenging because of low activity and weak long-term stability of anodic Pt electrocatalysts, as well as the high cost of precious metal Pt. Therefore, improving catalytic activity, stability and efficiency of anodic Pt electrocatalysts has currently been a pressing research topic in electrocatalysts development^{2,4–6,9,10}.

Untill now, various highly active Pt-based multi-metal nanostructures with the different structures, such as alloy^{3,11,12}, core-shell^{13,14} and heterostructure¹⁵ nanocrystals, have been synthesized successfully. Recently, there has been a growing interest in the synthesis of Pt-based multi-metal core-shell nanostructures consisting of nonprecious metal core (such as Ni@Pt^{16,17}) or less expensive noble metal core (such as Pd@Pt^{18–20} and Au@Pd@Pt^{13,14}). These Pt-based core-shell nanostructures with designed compositions and morphologies efficiently reduce the cost of Pt and synchronously improve Pt utilization. Meanwhile, these Pt-based core-shell nanostructures show the remarkably enhanced electrocatalytic activity and durability compared to single-component Pt electrocatalyst because of the geometric effect, electronic effect and synergistic effect between different components. For example, the Pd@Pt core-shell nanocrystals exhibited improved electrocatalytic activity and durability for the methanol oxidation reaction (MOR) compared to Pt nanodendrites and Pt nanocubes¹⁸. The Ni@Pt core-shell nanotube arrays exhibited higher electrocatalytic performance for the MOR compared to Pt/C catalyst¹⁶. To obtain core-shell nanostructures, many strategies have been developed successfully in the recent years. For instance, Li and co-workers utilized an epitaxial growth route to synthesize Pt@Pd nanocrystals with Na₃C₆H₅O₇ as a reductant at high temperature²¹. Koenigsmann and co-workers achieved Pd nanowire core@Pt monolayer shell nanostructures by Cu underpotential deposition followed by galvanic displacement of the Cu adatoms²². Yang and co-workers applied direct galvanic displacement to synthesize core-shell Pd@Pt/C electrocatalyst at high temperature²³.

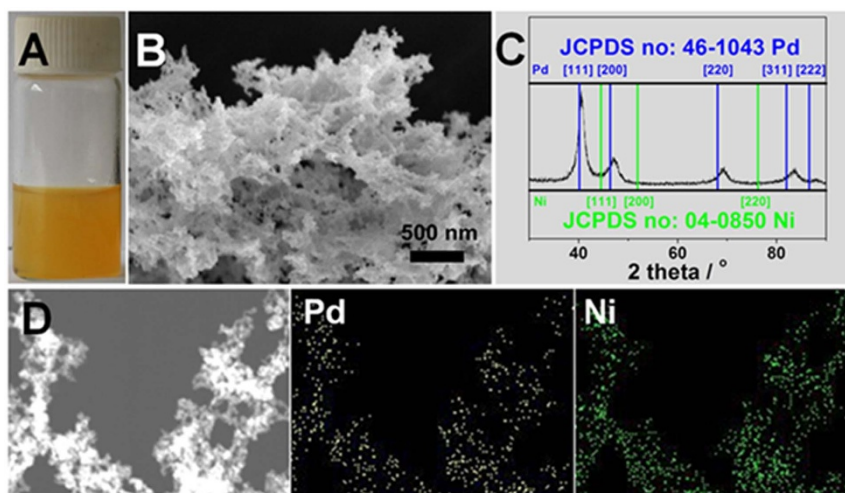


Figure 1 | (A) Photograph of $K_2PdCl_4/K_2Ni(CN)_4$ cyanogel. (B) SEM image, (C) XRD pattern, and (D) EDS elemental mapping patterns of Pd-Ni ANWs.

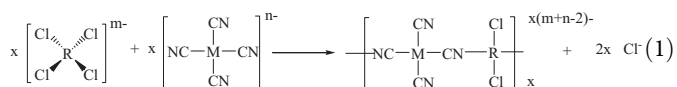
Besides structure, morphology of nanostructures plays an important role in determining their durability. For example, three-dimensionally (3D) porous morphology can contribute to remarkably enhanced electrocatalytic stability of nanostructures^{24–26}. Essentially, no individual nanoparticle exists in 3D porous nanostructures because of their interconnected structure, which effectively restrains Ostwald ripening effect and preserves their electrochemically surface areas (ECSA). In recent works, we have successfully synthesized the 3D porous noble metal nanostructures by reducing cyanogels with $NaBH_4$ at room temperature. The as-prepared 3D alloy nanostructures generally exhibited enhanced electrocatalytic activity and stability for the MOR, oxygen reduction reaction, ethanol oxidation reaction, and formic acid oxidation reaction, *etc.*^{27–30}.

Herein, we presented a facile aqueous synthesis of corallite-like PdNi@Pt core-shell nanostructures (PdNi@Pt CSNSs) with 3D porous morphology, which utilized Pd-Ni alloy networks (Pd-Ni ANWs) as a core component synthesized via cyanogel-reduction method, and further conducted the galvanic displacement with K_2PtCl_4 to generate Pt shell. Electrochemical measurements showed that PdNi@Pt CSNSs had the excellent electrocatalytic activity and stability for the MOR.

Results and Discussion

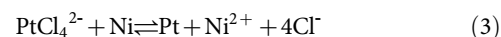
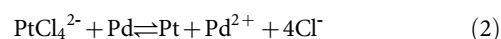
Synthesis of Pd-Ni alloy networks (Pd-Ni ANWs). Cyanogel, a coordinate inorganic polymer, is a special class of 3D double-metal cyanide, which can be easily achieved by mixing tetrachlorometalates ($[RCl_4]^{2-}$, $R=Sn, Pd, Pt$) and cyanometalates ($[M(CN)_n]^{2-/3-}$, ($n=4, 6$; $M= Pd, Pt, Fe, Co, Ni, Ru$) aqueous solutions (equation (1))^{27–33}. After mixing K_2PdCl_4 and $K_2Ni(CN)_4$ aqueous solutions at room temperature for 10 min, the orange jelly-like $K_2PdCl_4/K_2Ni(CN)_4$ cyanogel generates slowly (Figure 1A). In the inorganic polymer, Pd^{II} and Ni^{II} atoms uniformly mix and concentrate on the cyanogel's backbone. Once chemical reduction, the close connection between Pd^{II} and Ni^{II} species effectively facilitate the combination between Pd and Ni crystal nuclei. Moreover, the cyanogel's solid nature restrain the brownian motion of performed crystal nuclei, favouring the formation of Pd-Ni alloy. Furthermore, the 3D backbone of cyanogel can availably serve as a support scaffold to facilitate the formation of the interconnected 3D structure. Thus, the Pd-Ni alloy networks (Pd-Ni ANWs) can be conveniently achieved by cyanogel-reduction route with $NaBH_4$ (details see **Experimental Section**). As confirmed by scanning electron microscopy (SEM) image, the Pd-Ni products indeed have 3D network-like architectures (Figure 1B). X-ray diffraction (XRD) pattern demonstrates that Pd-Ni ANWs have

the face centered cubic (fcc) structure (Figure 1C). No diffraction peaks for single-component Pd or Ni is detected in the XRD pattern. Diffraction peaks at 40.62° , 47.17° , 69.17° , 83.58° and 88.03° shift to higher angle relative to Pd (JCPDS no: 04-1043) and to lower angle relative to Ni (JCPDS no: 04-0850), indicating the formation of Pd-Ni alloy³⁴. Energy dispersive spectrum (EDS) elemental mapping patterns display both Pt and Cu elements uniformly distributed in the whole Pd-Ni ANWs (Figure 1D), confirming the formation Pd-Ni alloy.



Synthesis of PdNi@Pt core-shell nanostructures (PdNi@Pt CSNSs).

Thanks to the discrepancy in the standard reduction potentials different metal couples ($E Ni^{2+}/Ni = -0.257 V$ vs. NHE, $E Pd^{2+}/Pd = 0.729 V$ vs. NHE, $E PtCl_4^{2-}/Pt = 1.249 V$ vs. NHE), PdNi@Pt core-shell nanostructures (CSNSs) can be easily obtained by the galvanic displacement reaction between Pd-Ni ANWs and K_2PtCl_4 in an aqueous solution at room temperature (equation (2) – (3)). In comparison with EDS spectrum of Pd-Ni ANWs (Figure S1A), the appearance of Pt element confirms the galvanic displacement reaction between Pd-Ni ANWs and K_2PtCl_4 (Figure S1B). EDS spectrum of PdNi@Pt CSNSs shows that the Pd/Ni/Pt atomic ratio is 61.2:22.6:16.2, in agreement with inductively coupled plasma atomic emission spectrometry (ICP-AES) data (62.0:21.4:16.6). Compared with Pd/Ni atomic ratio in Pd-Ni ANWs (68.0:32.0), the obvious decrease in Ni content indicates Ni element in Pd-Ni ANWs acts as a preferential reductant for the reduction of K_2PtCl_4 due to its stronger reduction capability than Pd.



The crystal structure of PdNi@Pt CSNSs was explored by XRD. XRD pattern of PdNi@Pt CSNSs shows typical fcc structure (Figure 2A-a), in consistent with XRD pattern of Pd-Ni ANWs (Figure 2A-b). On the one hand, typical XRD peak angles of Pd and Pt are very similar. On the other hand, the Pt shell with small particle size is difficultly detected by XRD. The two factors results in the high similarity in XRD patterns of PdNi@Pt CSNSs and Pd-Ni ANWs^{19,35,36}. Using Debye-Scherrer formula, the average particle size

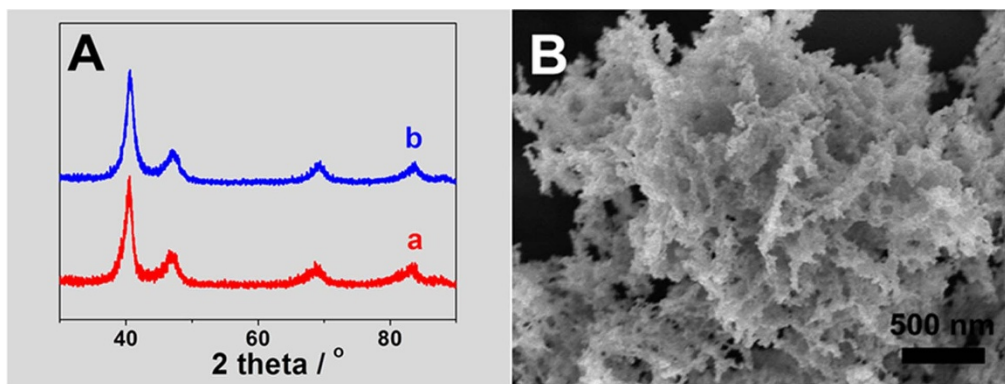


Figure 2 | (A) XRD patterns of (a) PdNi@Pt CSNs and (b) Pd-Ni ANWs. (B) SEM image of PdNi@Pt CSNs.

(d_{XRD}) of PdNi@Pt CSNs is calculated from {111} diffraction peak to be 5.9 nm, smaller than that of commercial Pt black ($d_{\text{XRD}} = 8.7$ nm, Figure S2). The morphology of PdNi@Pt CSNs was investigated by SEM. SEM image shows the products have the corallite-like 3D porous architectures (Figure 2B), very similar to the morphology of Pd-Ni ANWs (Figure 1B). Since such 3D architecture can essentially facilitate mass transport of fuel molecules, which is highly attractive for electrochemical applications.

The morphology and structural features of PdNi@Pt CSNs were further investigated by transmission electron microscopy (TEM). The large area TEM image shows PdNi@Pt CSNs consist of small and irregular nanoparticles, and these nanoparticles interconnect to generate abundant pores (Figure 3A). High-resolution TEM (HR-TEM) image shows the irregular interconnected nanostructures consist of ca. 7 nm grains (Figure 3B). Selected area electron diffraction (SAED) pattern displays a successive dotted pattern (insert in Figure 3B), demonstrating PdNi@Pt CSNs are polycrystalline. Magnified HRTEM image shows the lattice fringes with a spacing of 0.227 nm, in consistent with the Pt{111} facets (Figure 3C). The fast Fourier transform (FFT) pattern of the lattice image displays the diffraction spots with 6-fold rotational symmetry (inset in Figure 3C), confirming that PdNi@Pt CSNs are actually presented by {111} facets. Elemental mapping under scanning transmission electron microscopy mode is a powerful technique to investigate the element distribution of nanostructures. Clearly, the elemental distribution profiles of Pt, Pd and Ni are very similar (Figure 3D). And, EDS line scanning curves also confirm that Pt, Pd and Ni elements are evenly distributed through nanostructures (Figure 3E). But it is still hard to decide whether it is core-shell or alloy structures because the reduced Pt shell is a thin layer.

Fortunately, X-ray photoelectron spectroscopy (XPS) is a surface sensitive technique. XPS measurement shows the Pd : Ni : Pt atomic ratio in PdNi@Pt CSNs is 50.8 : 15.3 : 33.8 (Figure S3). Herein, the Pt content is noticeably higher than that measured by EDS (Pd : Ni : Pt atomic ratio is 61.2 : 22.6 : 16.2), demonstrating that PdNi@Pt core-shell nanostructures have been successfully synthesized. Further detailed analysis show the percentages of Pt⁰ and Pd⁰ species are 85.5% and 82.7%, respectively (Figure 4A–B), indicating metallic Pt and Pd are predominant in nanostructures. Compared with Pd-Ni ANWs, the Ni 2p signal at PdNi@Pt CSNs significantly weaken (Figure S4), confirming the galvanic displacement reaction between Ni and K₂PtCl₄ is predominant for the formation of PdNi@Pt CSNs. Meanwhile, the Pt 4f binding energies negatively shift ca. 0.15 eV relative to Pt black (Figure S5), which may be ascribed to the compressive strain introduced by PdNi substrate³⁷, and the electron donation induced by Pd and Ni with smaller electronegativity (Pt, 2.28; Pd, 2.20; Ni, 1.91)³⁸.

Methanol oxidation reaction. To study the coverage of Pt shell on PdNi@Pt CSNs, cyclic voltammetry (CV) tests were performed in

N₂-purged 0.5 M H₂SO₄ solution. As revealed by Figure 5A, the oxide reduction peak of PdNi@Pt CSNs (0.55 V) shifts positively ca. 90 mV compared to that of Pd-Ni ANWs (0.46 V), very close to that of Pt black (0.56 V), confirming a complete Pt shell has formed on Pd-Ni ANWs surface¹⁹. According to hydrogen adsorption–desorption method²⁷, the ECSA of PdNi@Pt CSNs and Pt black are measured to be 32.5, and 17.8 m² g⁻¹, respectively. The durabilities of PdNi@Pt CSNs and Pt black were investigated by continuous cyclic voltammetry running. After continuous 1000 cycles, PdNi@Pt CSNs and Pt black lost 13.5% and 32.5% of their initial ECSA, respectively (Figure 5B). Since PdNi@Pt CSNs keep the 3D interconnected structure from the core of Pd-Ni ANWs, the particular 3D structure effectively restrains Ostwald ripening effect^{24–26}, and contributes to an enhanced electrochemical stability.

The electrocatalytic activities of Pd-Ni ANWs, Pt black and PdNi@Pt CSNs for the MOR were investigated by CV in acidic media. No anodic current for the MOR is observed at Pd-Ni ANWs (Figure S6), indicating that Pd-Ni ANWs has no electrocatalytic activity for the MOR in acidic media. However, the obvious anodic peak for the MOR are found at both Pt black and PdNi@Pt

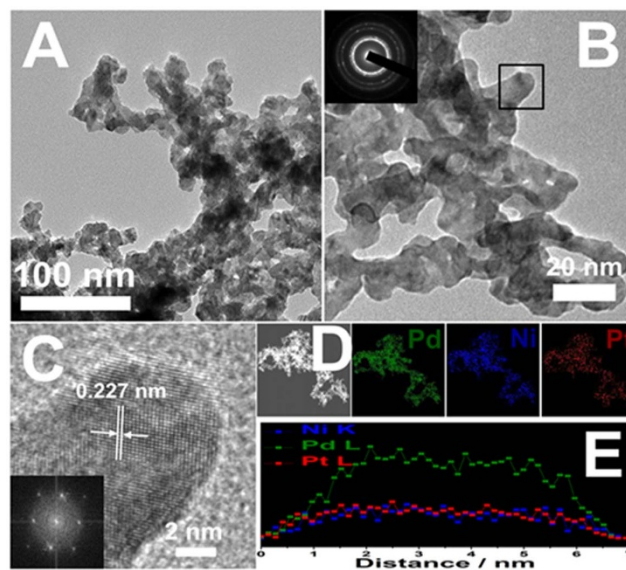


Figure 3 | (A) TEM image of PdNi@Pt CSNs. (B) HR-TEM image of PdNi@Pt CSNs. Inset: SAED pattern. (C) Magnified HR-TEM image taken from region marked by squares in Figure 3B. Inset: FFT pattern. (D) High angle angular dark field-scanning transmission electron microscopy image of PdNi@Pt CSNs and the corresponding EDS elemental mapping patterns. (E) EDS line scanning profiles of PdNi@Pt CSNs recorded from Figure 3D.

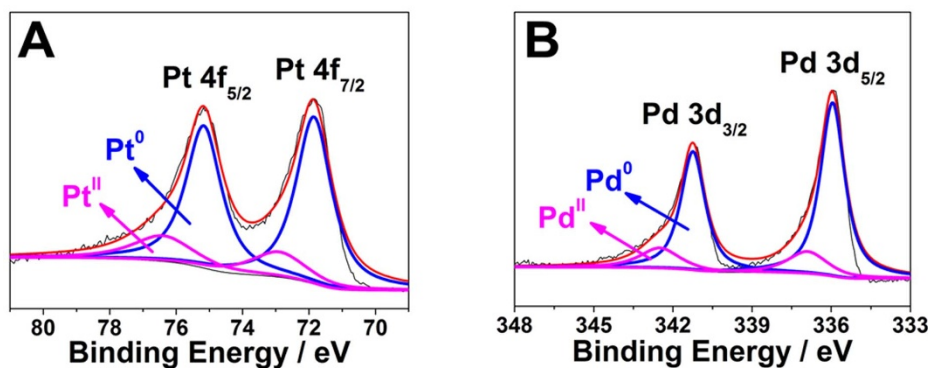


Figure 4 | (A) Pt 4f and (B) Pd 3d XPS spectra of PdNi@Pt CSNs.

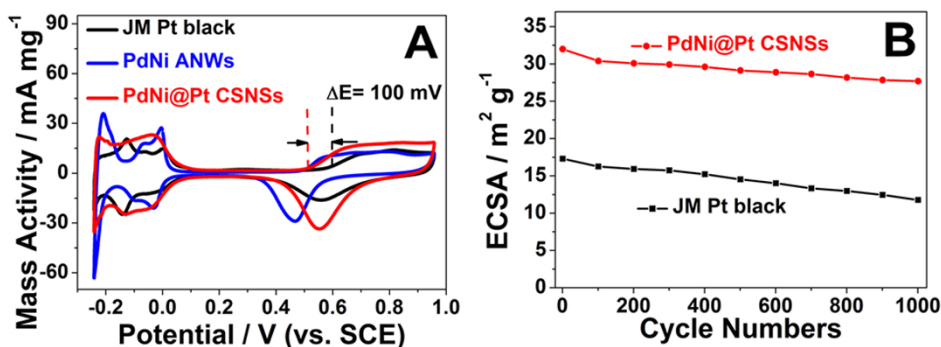


Figure 5 | (A) Cyclic voltammograms of PdNi@Pt CSNs, Pd-Ni ANWs and Pt black in N_2 -saturated 0.5 M H_2SO_4 solution at a sweep rate of 50 mV s^{-1} . (B) ECSA vs. cycle numbers of PdNi@Pt CSNs and Pt black.

CSNs (Figure 6A). The onset oxidation potential of the MOR at PdNi@Pt CSNs negatively shifts ca. 100 mV than that at Pt black, indicating that PdNi@Pt CSNs are more kinetically effective electrocatalysts. At 0.6 V potential, Pt mass activity on PdNi@Pt CSNs is 965 mA mg^{-1} , much higher than that on Pt black (161 mA mg^{-1}) and previous reports (such as Pt-Co alloy networks²⁷: 392 mA mg^{-1} , and FePtPd nanowires⁴: 450 mA mg^{-1}), indicating that the Pt utilization can be remarkably improved by using PdNi@Pt CSNs as electrocatalysts. Chronoamperometry technique was further carried out to investigate the electrocatalytic performance of electrocatalysts for the MOR (Figure 6B). The rate of current decay is exponential and after a long time a pseudo steady state is reached. In whole process, the MOR current on PdNi@Pt CSNs is higher than that on Pt black, showing their high activity. The long-term stability (δ) is

evaluated by measuring the linear current decay using the equation (4)²⁷:

$$\delta(\%s^{-1}) = \frac{100}{I_0} \times \left(\frac{dI}{dt} \right)_{t>500s} \quad (4)$$

Where I_0 is the at the start of polarization back extrapolated from the linear current decay, and $(dI/dt)_{t>500s}$ is the slope of the linear portion of the current decay. According to the equation (4), the loss rates of PdNi@Pt CSNs and Pt black MOR activities are 0.07 and $0.12\% \text{ s}^{-1}$, demonstrating that PdNi@Pt CSNs have an improved stability compared to Pt black.

Besides the effect of electrocatalyst's self-stability on durability, the effect of CO_{ads} poison on electrocatalyst's durability was also investigated by CO-stripping tests. In comparison with Pt black, the onset

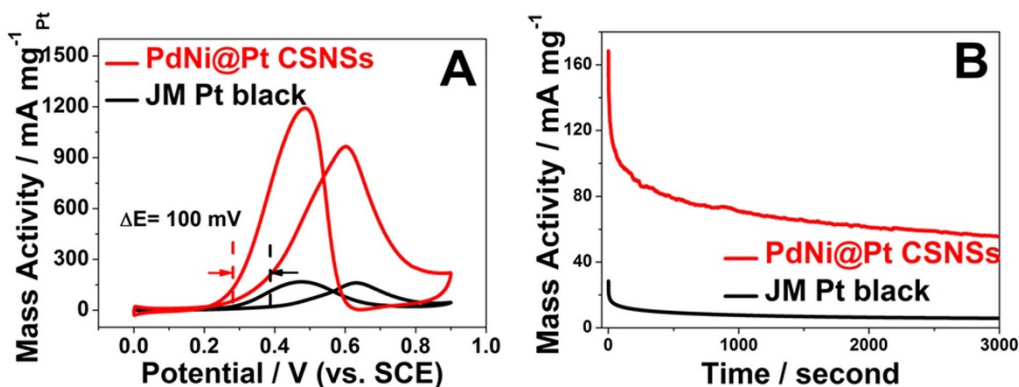


Figure 6 | (A) The Pt metal mass-normalized cyclic voltammograms for PdNi@Pt CSNs and Pt black in solution of 0.5 M methanol + 0.5 M H_2SO_4 at 50 mV s^{-1} . (B) Chronoamperometry curves for PdNi@Pt CSNs and Pt black in solution of 0.5 M methanol + 0.5 M H_2SO_4 for 3000 s at 0.6 V potential.

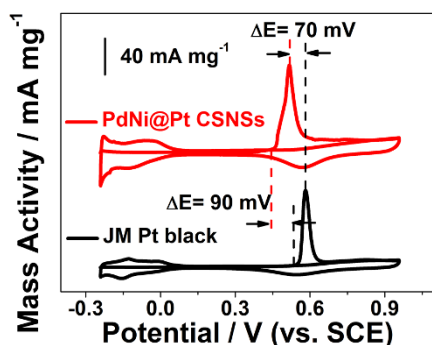


Figure 7 | Cyclic voltammograms of pre-adsorbed CO at PdNi@Pt CSNSs and Pt black modified electrodes in 0.5 M H₂SO₄ solution at 50 mV s⁻¹.

oxidation potential and oxidation peak potential of pre-adsorbed CO at PdNi@Pt CSNSs negatively shift ca. 90 and 70 mV, respectively (Figure 7). The result demonstrates that the PdNi core has a significant effect in changing the CO tolerance of electrocatalysts. According to the d-band center theory^{39,40}, the change in Pt 4f binding energy at PdNi@Pt CSNSs is responsible for effective removal of CO_{ads}, which contributes to improved durability for the MOR. Moreover, the PdNi core can be oxidized at lower potential than Pt shell to provide OH species, which also facilitates the valid removal of CO at PdNi@Pt CSNSs due to bifunctional mechanism.

In summary, we successfully synthesized the jelly-like K₂PdCl₄/K₂Ni(CN)₄ cyanogel. Due to 3D characteristic backbone and double-metal properties of the cyanogel, Pd-Ni ANWs were obtained facilely through a simple NaBH₄-reduction method at room temperature. This simple, mild and template-free cyanogel-reduction route was an attractive choice for the synthesis of the porous double metal alloy nanomaterials. Then, we utilized galvanic displacement to prepare PdNi@Pt CSNSs without any surfactant. Electrochemical measurements demonstrated that PdNi@Pt CSNSs showed enhanced electrocatalytic activity and durability for the MOR compared to Pt black, owing to the unique interconnected structure and the synergistic effect between PdNi core and Pt shell, such as electronic effect and bifunctional mechanism. This work demonstrated that PdNi@Pt CSNSs were indeed promising anodic electrocatalyst for the DMFCs.

Methods

Fabrication of PdNi ANWs and PdNi@Pt CSNSs. In a typical synthesis of PdNi ANWs, 4 mL of 50 mM K₂PdCl₄, and 2 mL of 50 mM K₂Ni(CN)₄ aqueous solutions were added into a 25-mL beaker for 10 min to generate the K₂PdCl₄/K₂Ni(CN)₄ cyanogel. Then 6 mL of 0.05 g mL⁻¹ NaBH₄ solution was dropwise added into the beaker and the K₂PdCl₄/K₂Ni(CN)₄ cyanogel was reacting violently to obtain the black Pd-Ni ANWs after 2 h. Afterwards separated with centrifugation at 18000 rpm for 8 min, dried in a vacuum oven at 45°C for 12 h, Pd-Ni ANWs were finally achieved. In a typical synthesis of PdNi@Pt CSNSs, 8 mg Pd-Ni ANWs were suspended in 20 mL water by ultrasonic concussion. Then, 0.5 mL of 0.05 M K₂PtCl₄ aqueous solution was added into Pd-Ni ANWs suspension at 60°C. After stirring for 6 h, the PdNi@Pt CSNSs were obtained and further separated by centrifugation at 18000 rpm for 8 min, and dried in a vacuum oven at 40°C overnight.

Characterization. The morphology and surface structure of samples were observed by JSM-2010 scanning electron microscopy (SEM) and JEOL JEM-2100F transmission electron microscopy (TEM). The composition and crystal structure of samples were investigated by energy dispersive spectrum (EDS) technique, Leeman inductively coupled plasma atomic emission spectrometry (ICP-AES), Thermo VG Scientific ESCALAB 250 X-ray photoelectron spectroscopy (XPS), and Model D/max-rC X-ray diffraction (XRD) diffractometer. The binding energy was calibrated by means of the C 1s peak energy of 284.6 eV.

Electrochemical tests. All electrochemical experiments were performed in an all-Teflon three-electrode cell by using a CHI 660 C electrochemical analyzer (CH Instruments, Shanghai, Chenghua Co.) at 30 ± 1°C. A platinum wire reacts as the auxiliary electrode, a saturated calomel electrode (SCE) reacts as reference electrode, and a catalyst modified glassy carbon electrode works as the working electrode. All potentials in this study were reported with respect to SCE. Working electrodes were

prepared by sonicating the catalyst powder in water at 1.4 mg mL⁻¹ for at least 1 h, and dispersing a 4 μL droplet onto a 3 mm glassy carbon electrode. The specific loading of total metal and Pt on the glassy carbon electrode (3 mm diameter) was about 80 μg cm⁻² and 13.3 μg cm⁻², respectively. CO-stripping tests were performed according to our previously reported procedure.

- Nassar, A. B. A. A., Sinev, I., Pohl, M.-M., Grünert, W. & Bron, M. Rapid microwave-assisted polyol reduction for the preparation of highly active PtNi/CNT electrocatalysts for methanol oxidation. *ACS Catal.* **4**, 2449–2462 (2014).
- Franceschini, E. A., Bruno, M. M., Williams, F. J., Viva, F. A. & Corti, H. R. High-activity mesoporous Pt/Ru catalysts for methanol oxidation. *ACS Appl. Mater. Interfaces* **5**, 10437–10444 (2013).
- Xia, B. Y., Wu, H. B., Wang, X. & Lou, X. W. One-pot synthesis of cubic PtCu₃ nanocages with enhanced electrocatalytic activity for the methanol oxidation reaction. *J. Am. Chem. Soc.* **134**, 13934–13937 (2012).
- Guo, S., Zhang, S., Sun, X. & Sun, S. Synthesis of ultrathin FePtPd nanowires and their use as catalysts for methanol oxidation reaction. *J. Am. Chem. Soc.* **133**, 15354–15357 (2011).
- Huang, H. & Wang, X. Recent progress on carbon-based support materials for electrocatalysts of direct methanol fuel cells. *J. Mater. Chem. A* **2**, 6266–6291 (2014).
- Chang, J., Feng, L., Liu, C., Xing, W. & Hu, X. Ni₂P enhances the activity and durability of the Pt anode catalyst in direct methanol fuel cells. *Energy Environ. Sci.* **7**, 1628–1632 (2014).
- Nguyen Viet, L. *et al.* The development of mixture, alloy, and core-shell nanocatalysts with nanomaterial supports for energy conversion in low-temperature fuel cells. *Nano Energy* **2**, 636–676 (2013).
- Tiwari, J. N., Tiwari, R. N., Singh, G. & Kim, K. S. Recent progress in the development of anode and cathode catalysts for direct methanol fuel cells. *Nano Energy* **2**, 553–578 (2013).
- Yin, A. X. *et al.* Pt-Cu and Pt-Pd-Cu concave nanocubes with high-index facets and superior electrocatalytic activity. *Chem. Eur. J.* **18**, 777–782 (2012).
- Rossmel, J. *et al.* Bifunctional anode catalysts for direct methanol fuel cells. *Energy Environ. Sci.* **5**, 8335–8342 (2012).
- Ding, L.-X. *et al.* Porous Pt-Ni-P composite nanotube arrays: highly electroactive and durable catalysts for methanol electrooxidation. *J. Am. Chem. Soc.* **134**, 5730–5733 (2012).
- Wang, L., Nemoto, Y. & Yamauchi, Y. Direct synthesis of spatially-controlled Pt-on-Pd bimetallic nanodendrites with superior electrocatalytic activity. *J. Am. Chem. Soc.* **133**, 9674–9677 (2011).
- Wang, L. & Yamauchi, Y. Autoprogrammed synthesis of triple-layered Au@Pd@Pt core-shell nanoparticles consisting of a Au@Pd bimetallic core and nanoporous Pt shell. *J. Am. Chem. Soc.* **132**, 13636–13638 (2010).
- Wang, L. & Yamauchi, Y. Strategic synthesis of trimetallic Au@Pd@Pt core-shell nanoparticles from poly(vinylpyrrolidone)-based aqueous solution toward highly active electrocatalysts. *Chem. Mater.* **23**, 2457–2465 (2011).
- Wu, J., Hou, Y. & Gao, S. Controlled synthesis and multifunctional properties of FePt-Au heterostructures. *Nano Res.* **4**, 836–848 (2011).
- Ding, L.-X. *et al.* Porous Ni@Pt core-shell nanotube array electrocatalyst with high activity and stability for methanol oxidation. *Chem. Eur. J.* **18**, 8386–8391 (2012).
- Chen, Y., Yang, F., Dai, Y., Wang, W. & Chen, S. Ni@Pt core-shell nanoparticles: synthesis, structural and electrochemical properties. *J. Phys. Chem. C* **112**, 1645–1649 (2008).
- Kim, Y., Lee, Y. W., Kim, M. & Han, S. W. One-pot synthesis and electrocatalytic properties of Pd@Pt core-shell nanocrystals with tailored morphologies. *Chem. Eur. J.* **20**, 7901–7905 (2014).
- Zhang, H. *et al.* Pd@Pt core-shell nanostructures with controllable composition synthesized by a microwave method and their enhanced electrocatalytic activity toward oxygen reduction and methanol oxidation. *J. Phys. Chem. C* **114**, 11861–11867 (2010).
- Li, S.-S. *et al.* Facile synthesis of PdPt@Pt nanorings supported on reduced graphene oxide with enhanced electrocatalytic properties. *ACS Appl. Mater. Interfaces* **6**, 10549–10555 (2014).
- Li, Y. *et al.* Synthesis of bimetallic Pt-Pd core-shell nanocrystals and their high electrocatalytic activity modulated by Pd shell thickness. *Nanoscale* **4**, 845–851 (2012).
- Koenigsmann, C. *et al.* Enhanced electrocatalytic performance of processed, ultrathin, supported Pd-Pt core-shell nanowire catalysts for the oxygen reduction reaction. *J. Am. Chem. Soc.* **133**, 9783–9795 (2011).
- Yang, J., Lee, J. Y., Zhang, Q., Zhou, W. & Liu, Z. Carbon-supported pseudo-core-shell Pd-Pt nanoparticles for ORR with and without methanol. *J. Electrochem. Soc.* **155**, B776–B781 (2008).
- Xia, B. Y., Ng, W. T., Bin Wu, H., Wang, X. & Lou, X. W. Self-supported interconnected Pt nanoassemblies as highly stable electrocatalysts for low-temperature fuel cells. *Angew. Chem. Int. Ed.* **51**, 7213–7216 (2012).
- Sun, S. H. *et al.* A highly durable platinum nanocatalyst for proton exchange membrane fuel cells: multiarmed starlike nanowire single crystal. *Angew. Chem. Int. Ed.* **50**, 422–426 (2011).
- Mourdikoudis, S. *et al.* Dimethylformamide-mediated synthesis of water-soluble platinum nanodendrites for ethanol oxidation electrocatalysis. *Nanoscale* **5**, 4776–4784 (2013).



27. Xu, J. *et al.* Platinum-cobalt alloy networks for methanol oxidation electrocatalysis. *J. Mater. Chem.* **22**, 23659–23667 (2012).
28. Zhang, G. *et al.* Synthesis and electrocatalytic properties of palladium network nanostructures. *ChemPlusChem* **77**, 936–940 (2012).
29. Liu, X. *et al.* Pt-Pd-Co trimetallic alloy network nanostructures with superior electrocatalytic activity towards the oxygen reduction reaction. *Chem. Eur. J.* **20**, 585–590 (2014).
30. Liu, X.-Y. *et al.* Facile synthesis of corallite-like Pt–Pd alloy nanostructures and their enhanced catalytic activity and stability for ethanol oxidation. *J. Mater. Chem. A* **2**, 13840–13844 (2014).
31. Vondrova, M., McQueen, T. M., Burgess, C. M., Ho, D. M. & Bocarsly, A. B. Autoreduction of Pd–Co and Pt–Co cyanogels: exploration of cyanometalate coordination chemistry at elevated temperatures. *J. Am. Chem. Soc.* **130**, 5563–5572 (2008).
32. Burgess, C. M., Vondrova, M. & Bocarsly, A. B. A versatile chemical method for the formation of macroporous transition metal alloys from cyanometalate coordination polymers. *J. Mater. Chem.* **18**, 3694–3701 (2008).
33. Pfennig, B. W., Bocarsly, A. B. & Prud'homme, R. K. Synthesis of a novel hydrogel based on a coordinate covalent polymer network. *J. Am. Chem. Soc.* **115**, 2661–2665 (1993).
34. Park, K.-W., Sung, Y.-E., Han, S., Yun, Y. & Hyeon, T. Origin of the enhanced catalytic activity of carbon nanocoil-supported PtRu alloy electrocatalysts. *J. Phys. Chem. B* **108**, 939–944 (2003).
35. Lan, F. *et al.* Ultra-low loading Pt decorated coral-like Pd nanochain networks with enhanced activity and stability towards formic acid electrooxidation. *J. Mater. Chem. A* **1**, 1548–1552 (2013).
36. Peng, Z. & Yang, H. Synthesis and oxygen reduction electrocatalytic property of Pt-on-Pd bimetallic heteronanostructures. *J. Am. Chem. Soc.* **131**, 7542–7543 (2009).
37. Yang, J., Zhou, W., Cheng, C. H., Lee, J. Y. & Liu, Z. Pt-decorated PdFe nanoparticles as methanol-tolerant oxygen reduction electrocatalyst. *ACS Appl. Mater. Interfaces* **2**, 119–126 (2009).
38. Zhang, G. *et al.* Aqueous-phase synthesis of sub 10 nm Pd@Pt shell nanocatalysts for oxygen reduction reaction using amphiphilic triblock copolymers as the reductant and capping agent. *J. Phys. Chem. C* **117**, 13413–13423 (2013).
39. Hammer, B. & Nørskov, J. Electronic factors determining the reactivity of metal surfaces. *Surf. Sci.* **343**, 211–220 (1995).
40. Hammer, B., Morikawa, Y. & Nørskov, J. K. CO chemisorption at metal surfaces and overlayers. *Phys. Rev. Lett.* **76**, 2141–2144 (1996).

Acknowledgments

This research was sponsored by National Natural Science Foundation of China (21473111, 21376122 and 21273116), Natural Science Foundation of Jiangsu Province (BK20131395), United Fund of NSFC and Yunnan Province (U1137602), Industry-Academia Cooperation Innovation Fund Project of Jiangsu Province (BY2012001), the National Basic Research Program of China (973 Program, 2012CB215500), Fundamental Research Funds for the Central Universities (GK201402016) and a project funded by the Priority Academic Program Development of Jiangsu Higher Education Institutions.

Author contributions

X.L. and G.X. designed the experiments and performed the materials synthesis, characterization and electrochemical measurements. Y.T. and Y.C. wrote the main manuscript text. T.H. and W.X. supervised the project, and all authors participated in the review of the manuscript.

Additional information

Supplementary information accompanies this paper at <http://www.nature.com/scientificreports>

Competing financial interests: The authors declare no competing financial interests.

How to cite this article: Liu, X. *et al.* A Strategy for Fabricating Porous PdNi@Pt Core-shell Nanostructures and Their Enhanced Activity and Durability for the Methanol Electrooxidation. *Sci. Rep.* **5**, 7619; DOI:10.1038/srep07619 (2015).



This work is licensed under a Creative Commons Attribution-NonCommercial-NoDerivs 4.0 International License. The images or other third party material in this article are included in the article's Creative Commons license, unless indicated otherwise in the credit line; if the material is not included under the Creative Commons license, users will need to obtain permission from the license holder in order to reproduce the material. To view a copy of this license, visit <http://creativecommons.org/licenses/by-nc-nd/4.0/>